

# Depth profile study of $^{210}\text{Pb}$ in the surface of an NaI(Tl) crystal

G. H. Yu<sup>a</sup>, C. Ha<sup>b</sup>, E. J. Jeon<sup>b,\*</sup>, K. W. Kim<sup>b,\*</sup>, N.Y. Kim<sup>b</sup>, Y. D. Kim<sup>b,c,d</sup>, H. S. Lee<sup>b,d</sup>, H.K. Park<sup>e</sup>, C. Rott<sup>a</sup>

<sup>a</sup>Department of Physics, Sungkyunkwan University, Suwon 16419, South Korea

<sup>b</sup>Center for Underground Physics, Institute for Basic Science (IBS), Daejeon 34126, South Korea

<sup>c</sup>Department of Physics, Sejong University, Seoul 05006, South Korea

<sup>d</sup>IBS School, University of Science and Technology (UST), Daejeon 34113, South Korea

<sup>e</sup>Department of Accelerator Science, Korea University, Sejong 30019, South Korea

## Abstract

The surface  $^{210}\text{Pb}$  is one of the main background sources for dark-matter-search experiments using NaI(Tl) crystals, and its spectral features associated with the beta-decay events for energies less than 60 keV depends on the depth distribution of  $^{210}\text{Pb}$  in the surface of an NaI(Tl) crystal. Therefore, we must understand the profile of surface  $^{210}\text{Pb}$  to precisely model the background measurement in the low-energy region for the low-background experiment using NaI(Tl) crystals. We estimate the depth profile of the surface  $^{210}\text{Pb}$  contamination by modeling the measured spectrum of the alpha emission from the decay of  $^{210}\text{Po}$  at the decay sequence of the surface  $^{210}\text{Pb}$  contamination that is obtained using an  $^{222}\text{Rn}$ -contaminated crystal. In order to describe the energy spectra of the surface contamination we perform a log-likelihood fit of the measured data to a sum of Geant4 Monte Carlo simulations, weighted by an exponential curve as a function of the surface depth. The low- and high-energy events from the beta decay of surface  $^{210}\text{Pb}$  are also modeled to improve the depth profile for shallow depths. We simulate the energy spectra from beta decays of  $^{210}\text{Pb}$  that are exponentially distributed in the surface by following two exponential functions where the mean-depth coefficients are free parameters in the data fitting; we observed that the energy spectra are in good agreement with the measured data.

**Keywords:** Surface contamination, depth profile,  $^{210}\text{Pb}$ ,  $^{210}\text{Po}$ , NaI(Tl) crystal

## 1. Introduction

The presence of dark-matter particles in the Universe has been evidenced via numerous astronomical observations [1, 2]. Weakly interacting massive particles (WIMPs) are one of the most attractive candidates for being dark-matter particles [3, 4]. Many experiments have been conducted for directly searching WIMPs in our galaxy by looking for nuclear recoils that are produced by WIMP–nucleus scattering [5, 6]; however null results have been reported thus far with a notable exception, the DAMA/LIBRA experiment, which has consistently reported the observation of an annual event-rate modulation in an array of NaI(Tl) crystal detectors; this modulation, with a statistical significance of more than  $12.9\sigma$  [14, 15], could be interpreted as a dark-matter signal [7]. Furthermore, there are several NaI(Tl)-crystal-based experiments [8, 9, 10, 11, 12, 13] to test DAMA/LIBRA’s observation of an annual event-rate modulation.

Searching an annual modulation signal requires the complete understanding of background sources and complete simulation that accurately models the background-energy

spectra measured using the detector; therefore, background models, which are based on Monte Carlo simulations, have been built using the Geant4 toolkit [16] [17, 18, 19, 20, 21, 22]. In these models, it has been reported that the low-energy contribution from the beta-decay of  $^{210}\text{Pb}$  in the surface of NaI(Tl) crystals is one of the dominant background sources; furthermore, it has been suggested that sources are attributed to the  $^{222}\text{Rn}$  contamination that occurred anytime during the powder- and/or crystal-processing stages [17, 18, 20, 21].

As depicted in Fig. 1, the short-lived  $^{222}\text{Rn}$  decays to  $^{218}\text{Po}$ , which can be deposited on the crystal surface as a reactive metal and recoils  $^{214}\text{Pb}$  into the crystal surface during its subsequent alpha decay [23, 24]. The  $^{214}\text{Po}$  alpha decay after the beta decays of  $^{214}\text{Pb}$  results in the implantation of  $^{210}\text{Pb}$  deeper into the surface; consequently,  $^{210}\text{Pb}$  has an implanted distribution in the surface and also a long half-life ( $t_{1/2} = 22.3$  years), thereby acting as a background source for the low-energy region in an NaI(Tl) crystal; in addition, it contributes to the low-energy spectra by the beta decays to  $^{210}\text{Bi}$ , which decays to  $^{210}\text{Po}$  and subsequently, decays via alpha emission to  $^{206}\text{Pb}$ .

Because the beta decay to  $^{210}\text{Bi}$  results in low-energy events via the emissions of electrons and  $\gamma$ /X-ray, the spectral features of these events for energies less than 60 keV depend on the depth distribution of  $^{210}\text{Pb}$  within

\*Corresponding authors

Email addresses: ejjeon@ibs.re.kr (E. J. Jeon),  
kwkim@ibs.re.kr (K. W. Kim)

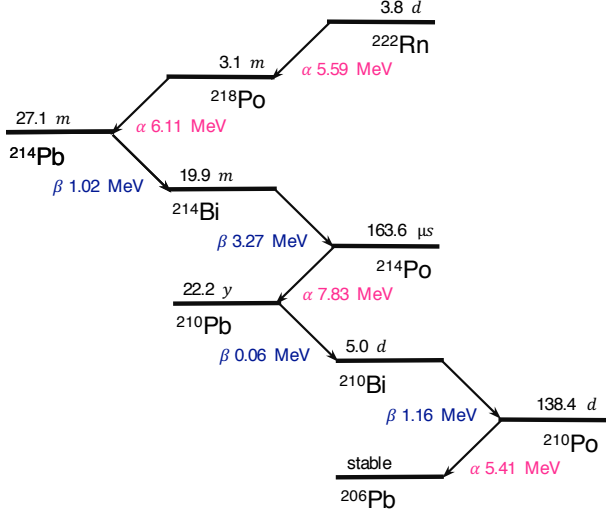


Figure 1:  $^{222}\text{Rn}$  decay chain. Alpha-decay Q values (down-left arrow), beta-decay Q values (down-right arrow), and half-lives are indicated.

the crystal surface. Therefore, we must completely understand the surface  $^{210}\text{Pb}$  profile to precisely model the background measurement in the low-energy region for low-background experiments using NaI(Tl) crystals. Additionally, there are other experiments not using NaI(Tl) crystals that improved the techniques to reject the surface background [25, 26, 27].

To estimate the depth profile of the surface  $^{210}\text{Pb}$  contamination, we model the measured spectrum due to the alpha emission from the decay of surface  $^{210}\text{Po}$  ( $t_{1/2} = 138$  days) at the decay sequence of surface  $^{210}\text{Pb}$  ( $t_{1/2} = 22.3$  years), by performing Monte Carlo simulations using the Geant4 version 10.4.p02 (Sect. 3). In addition, the low- and high-energy events from the beta decay of surface  $^{210}\text{Pb}$  are modeled to improve the depth profile for shallow depths (see Sect. 4).

## 2. Experimental setup

A copper encapsulated cylindrical NaI(Tl) crystal - with 8 cm diameter, 10 cm length, and 1.28 kg mass - was used in the experiment. It was made using the same ingot as the two crystals (C6 and C7) employed in the COSINE-100 experiment and encapsulated with the same copper that was used for the COSINE-100 crystals [28, 29]. The crystal was cut into two pieces, and the surface of one piece (Crystal B) was exposed to  $^{222}\text{Rn}$  gas from a  $^{226}\text{Ra}$  source for two weeks, while the other piece (Crystal A) was retained as clean. Subsequently, both the pieces were attached facing each other by inserting a 4- $\mu\text{m}$  thick aluminized mylar film between them; the film not allowed scintillation photons of a few eV to pass through it. In addition, two photomultiplier tubes (PMTs), which detected

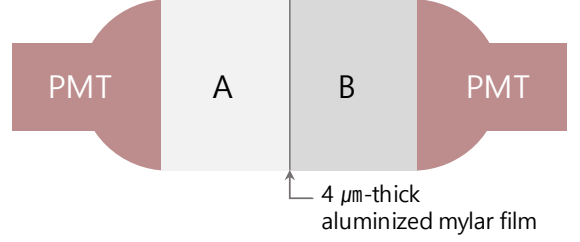


Figure 2: Schematic view of the detector. The crystal was cut into two pieces, and one of the pieces, i.e., Crystal B, was exposed to a radon source, while the other piece, i.e., Crystal A, was retained as clean. Subsequently, both the pieces were joined by inserting a 4- $\mu\text{m}$  thick mylar film, which allowed alpha particles to pass through it but no optical photons.

the scintillation signals coming from the crystals, were attached at the ends of both the crystal. The signal was saved only when the height of the pulse in both the PMTs was greater than the preset threshold. Figure 2 depicts the crystal-PMT detector module, which was installed inside the CsI(Tl) crystal array setup that had been previously deployed in the KIMS experiment in Yangyang underground laboratory [30]. Furthermore, Nitrogen gas was supplied into the detector setup to avoid radon contamination and maintain a stable humidity level; the details of the experimental setup and data-recording conditions are described in Ref. [31].

To minimize the contributions from the decay of the mother isotopes of  $^{210}\text{Pb}$  and to ensure events primarily from the  $^{210}\text{Pb}$  decay, only the data recorded after 70 days from the date of detector installation were used in this study; notably, the amount of data corresponds to 110 days. The data were prepared using the following criteria. An event that has hits only in the NaI(Tl) crystals (Crystals A and B) is called a single-hit event, whereas the one that has accompanying hits in the surrounding CsI(Tl) crystals too is called a multiple-hit event. For this study, we selected single-hit events since multiple-hit events are mostly due to external background sources. In addition, a timing coincidence within 200 ns was required between Crystals A and B, called coincidence events, to consider the events that were mainly induced by the deposition on the crystal surface. Furthermore, the energy scale below 100 keV was calibrated using a  $\gamma$ -ray source and the background spectra from several radioactivities of each crystal. For Crystal A, we used the peaks at 12, 28, and 46.5 keV from the surface  $^{210}\text{Pb}$ , and at 59.54 keV from a  $^{241}\text{Am}$   $\gamma$ -ray source. The peak at 76.63 keV contributed by X-rays from the decays of  $^{214}\text{Pb}$  and  $^{214}\text{Bi}$  was used for Crystal B. Above 100 keV, energy calibration was performed using peaks at 609 and 1120 keV from  $^{214}\text{Bi}$  for both the NaI(Tl) crystals.

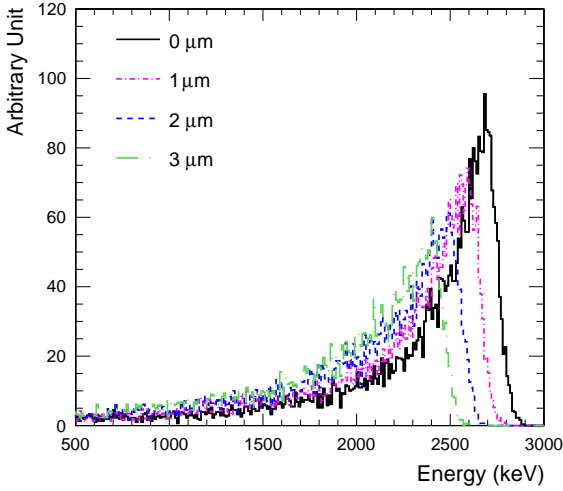


Figure 3: Simulated alpha energy spectra deposited in Crystal A according to various depths of the surface of Crystal B. We used the 5.3 MeV alpha energy from the decay of  $^{210}\text{Po}$ , considering 59% of  $\alpha/\beta$  light ratio at a given energy and assumed linearly quenched alphas, as determined by DAMA [32]. The property that the spectrum changes according to the depth position allows us to profile the depth-distribution with alpha spectrum.

### 3. Modeling alpha spectra of $^{210}\text{Po}$ decay in the crystal surface

#### 3.1. Simulations of the surface $^{210}\text{Po}$ contamination

As described in Sect. 2, the surface of Crystal B was exposed to  $^{222}\text{Rn}$  gas from a  $^{226}\text{Ra}$  source for two weeks; therefore,  $^{210}\text{Pb}$  at the decay sequence of  $^{222}\text{Rn}$  exhibits an implanted distribution in the surface with a long half-life ( $t_{1/2} = 22.3$  years); it results in a low-energy spectra because of the beta decays to  $^{210}\text{Po}$ , which subsequently decays via alpha emission to  $^{206}\text{Pb}$ . To estimate the depth profile of the surface  $^{210}\text{Pb}$  contamination, we modeled the spectrum measured by the clean crystal, i.e., Crystal A; the spectrum is attributed to the alpha emission from the decay of surface  $^{210}\text{Po}$  ( $t_{1/2} = 138$  days) of the contaminated Crystal B, by simulating all the decay chains of  $^{210}\text{Pb}$  with origin in the surface of Crystal B. We, thus, generated  $^{210}\text{Pb}$  through different depths of the surface of Crystal B, and investigated the correlation of alpha spectra measured using clean Crystal A in terms of the surface depth. Because of both the thin mylar layer and the small energy depositions on the contaminated crystal, i.e., Crystal B, the measured energy of the alpha particles was below the full energy deposition of  $^{210}\text{Po}$ , as reported in Ref. [31]; in addition, their small energy depositions on Crystal B vary depending on the depth of the contamination, thereby resulting in different alpha spectra on clean Crystal A, as depicted in Fig. 3. These were used as inputs when fitting the measured data to the sum of these MC spectrums, weighted by an exponential curve as a function of the contamination depth; the details are described in Sect. 3.2.

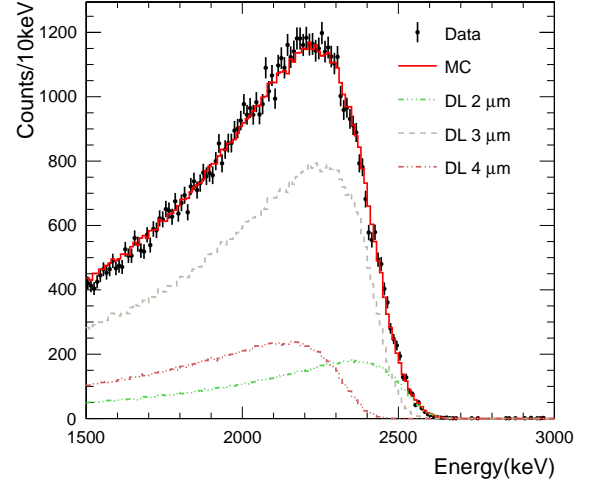


Figure 4: Comparison of data and fitted result for the alpha spectrum on the clean Crystal A.

To compare the energy spectrum of the alpha particles from the simulations with the data, we used the 5.3 MeV alpha energy from the decay of  $^{210}\text{Po}$  that is measured to be  $3.126 \pm 0.008$  MeV electron equivalent energy in the clean Crystal A, corresponding to 59% of light ratio at 5.3 MeV. This value is in good agreement with the quenching factor measured by DAMA at this energy [32], so in the following we assume the same energy dependence as in Ref. [32]. Upon contaminating a crystal by exposing it to  $^{222}\text{Rn}$  gas, a foggy layer was formed on its surface; this layer can affect the scintillation performance by acting as an inactive region or a dead layer (DL) [33]; therefore, the contaminated crystal, i.e., Crystal B, appeared obscured, while the clean Crystal A appeared transparent. We, thus, considered a DL of variable thickness in the surface of contaminated Crystal B.

#### 3.2. Results and comparison with measured data

To model the surface  $^{210}\text{Pb}$  spectrum, we generated  $^{210}\text{Pb}$  decays at random locations within the surface thickness of  $10 \mu\text{m}$  in the contaminated Crystal B, which was divided into 100 bins, each with a thickness of  $0.1 \mu\text{m}$ , to control the fraction of events on the basis of depth. We assume that they are exponentially distributed in the surface and the energy spectrum deposited in Crystal A,  $N(E)$ , is as follows:

$$N(E) = p_0 \sum_{DL=0}^5 F_{DL} \sum_{d=0}^{10\mu\text{m}} N_d^{DL}(E) \exp\left(\frac{-d}{p_1}\right) \quad (1)$$

where  $F_{DL}$  represents the fraction of the dead layer of thickness  $DL \mu\text{m}$ ,  $d$  denotes the contamination depth in  $\mu\text{m}$ ,  $N_d^{DL}(E)$  the energy spectra deposited in Crystal A by the events generated at the surface depth  $d$  for every  $DL$ , and  $p_0$  and  $p_1$  the amplitude and mean depth of the exponential distribution, respectively. Subsequently,

we fitted the alpha spectrum measured using the clean Crystal A by employing the log likelihood method, which allows the simulated spectrum to follow Eq. (1), with free-floating parameters  $p_0$ ,  $p_1$ , and  $F_{DL}$ . In the fit, we included five DLs (DL1, DL2, DL3, DL4, and DL5) of various thicknesses from 1 to 5  $\mu\text{m}$  as follows: 0~1, 0~2, 0~3, 0~4, and 0~5  $\mu\text{m}$ , and their fractions were treated as free-floating parameters. DL0 represents no dead layer. Figure 4 depicts the fitted result (solid red line) for the alpha spectrum on the clean Crystal A; the result is in good agreement with the data (filled black circles). The result supports a  $^{210}\text{Po}$  distribution following an exponential function with best fit parameters,  $p_1 = (1.39 \pm 0.02) \mu\text{m}$  and the fractions of dead layers that are 0%, 0%, 5.5%, 56.2%, 38.2%, and 0% for DL0, DL1, DL2, DL3, DL4, and DL5, respectively. The area under the DL4 curve shown in Fig. 4 is slightly larger than that of DL2 while the fractions of DL2 and DL4 are resulted in 5.5% and 38.2% from the fit. It is because less events are tagged as coincidence events when they are simulated including a thick dead layer. Accordingly, it shows that the alpha-decay events from  $^{210}\text{Po}$  generated on the surface for the DLs with thicknesses of 3 and 4  $\mu\text{m}$  are dominant contributors.

#### 4. Modeling the energy spectra of $^{210}\text{Pb}$ beta decay within the crystal surface

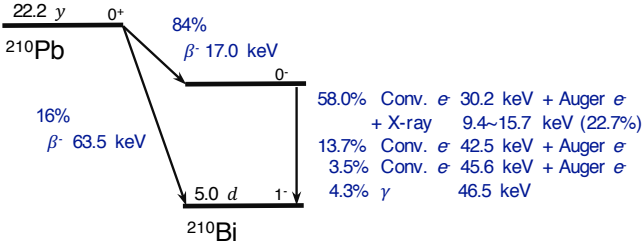


Figure 5: Beta decays of  $^{210}\text{Pb}$ .

As shown in Fig. 5, the beta decays to  $^{210}\text{Bi}$  from  $^{210}\text{Pb}$  produced low-energy events via the emissions of electrons and  $\gamma$ /X-ray; therefore, their spectral features for energies less than 60 keV depend on the depth distribution of  $^{210}\text{Pb}$  on the crystal surface. To understand the energy spectra from the beta decays of  $^{210}\text{Pb}$ , we simulated them by generating  $^{210}\text{Pb}$  at random locations within the surface thickness of 1  $\mu\text{m}$  in Crystal B. The simulated spectra for both the contaminated Crystal B and clean Crystal A are depicted in Fig. 6 (a) and (b), where each color represents the beta decays of  $^{210}\text{Pb}$  (dotted red line) and  $^{210}\text{Bi}$  (dashed blue line), respectively. The peaks at approximately 10 and 46 keV are attributed to the X-rays and 46.5 keV  $\gamma$ -ray from the decays of  $^{210}\text{Pb}$ . In addition, the conversion electrons contribute to the peaks at approximately 20 and 35 keV. Therefore, these spectral features

depend on the beta-decay events distributed within a shallow surface depth.

To verify the depth profile derived using the alpha-spectrum model, which is described in Sect. 3.2, we compared the low-energy spectra measured using each of Crystals A and B with the simulated spectra of  $^{210}\text{Pb}$  that is distributed in the surface of Crystal B, in accordance with the depth profile derived using the alpha spectrum; we observed that the low-energy spectra were not satisfactorily reproduced using the simulated spectra in the low-energy region, as depicted in Fig. 7 (solid red line). To avoid the randomly coincident events in the low energy region due to the backgrounds and noise in the  $^{222}\text{Rn}$ -contaminated Crystal B and Crystal A, we do not use those events below 5 keV in the clean Crystal A and 15 keV in the contaminated Crystal B, respectively.

If the  $^{210}\text{Po}$  contamination is zero at the moment when the initial  $^{210}\text{Pb}$  contamination occurred, it will grow with the  $^{210}\text{Po}$  half-life, i.e.,  $\tau_{Po210} = 138$  days, until reaching an equilibrium. This change in the total alpha rate with time can provide information regarding the total amount of the surface  $^{210}\text{Pb}$  contamination. Because the 110 day data used in this study were recorded after 70 days from the time when the initial  $^{210}\text{Pb}$  contamination occurred and when an equilibrium was not yet reached, the  $^{210}\text{Po}$  contamination is lower than the surface  $^{210}\text{Pb}$  contamination. However, the spectral feature of the simulation is not satisfactorily matched to the data, even when scaled, as shown in the dotted red line of Fig. 7. The spectral feature discrepancy between the data and simulation can be explained as follows: most alpha events occurring at the shallow depth of less than 1  $\mu\text{m}$  are not tagged as coincidence events when it is dominated by an inactive region and when the path length of the recoiled  $^{206}\text{Pb}$  with 106 keV kinetic energy is as small as  $\sim 50$  nm; therefore, it results in the lack of full understanding of the depth profile for shallow depths.

Therefore, to improve the model for better understanding the depth profile of  $^{210}\text{Pb}$  for shallow depths, we assume that they are exponentially distributed in the surface of Crystal B, via following two exponential functions:

$$N(E) = \sum_{DL=0}^5 F_{DL} \left[ p_0 \sum_{d=0}^{10\mu\text{m}} N_d^{DL}(E) \exp\left(\frac{-d}{p_1}\right) + p_2 \sum_{d=0}^{10\mu\text{m}} N_d^{DL}(E) \exp\left(\frac{-d}{p_3}\right) \right] \quad (2)$$

where we constrain the parameters  $p_1$  and  $F_{DL}$  using  $(1.39 \pm 0.02) \mu\text{m}$  and the fractions of dead layers obtained from the alpha spectrum modeling described in Sect. 3.2 and treat  $p_0$ ,  $p_2$ , and  $p_3$  as free-floating parameters in the data fitting. In the fit, the low- and high-energy spectra of the beta-decay events, as well as the energy deposited in each of Crystals A and B, are simultaneously fitted using simulations. The fitted energy spectra for both Crystals A and B (solid red line) are compared with the measure-

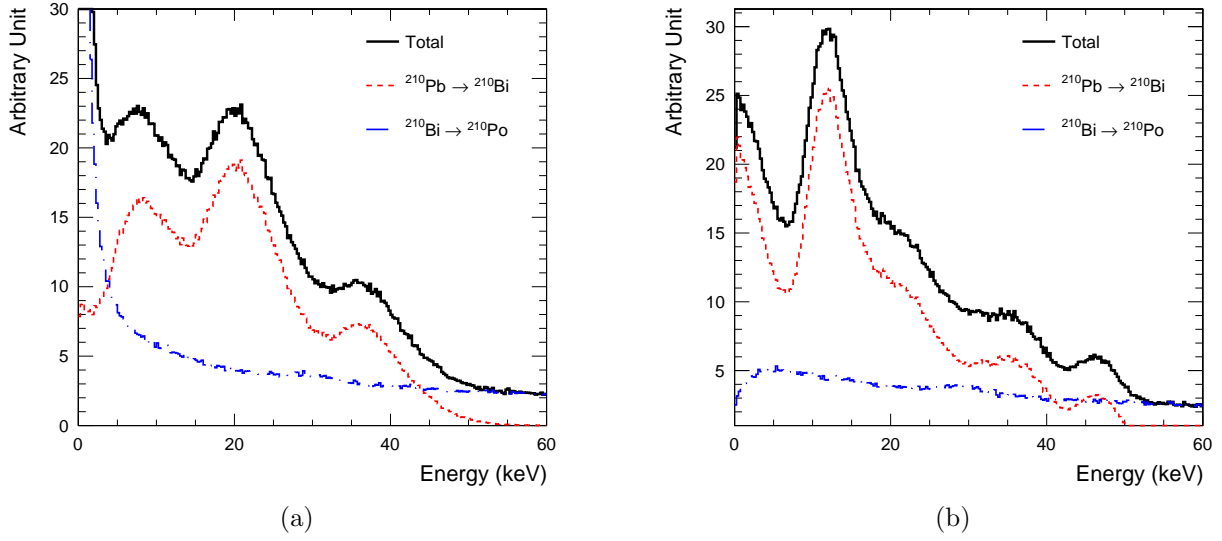


Figure 6: Low-energy spectra due to the beta decay of  $^{210}\text{Pb}$  to  $^{210}\text{Po}$ : in the contaminated Crystal B (a), and in the clean Crystal A (b).

ment results (filled black circles), as depicted in Fig. 8. The overall energy spectra (solid red lines) for both the clean Crystal A and contaminated Crystal B are in a good agreement with the data, not only for low-energy events but also for high-energy events. The high-energy events are dominantly the result of the external  $^{226}\text{Ra}$  from the copper cylinder that encapsulates the NaI(Tl) crystal that

also slightly contributes to the low-energy region and beta decay from  $^{210}\text{Bi}$  to  $^{210}\text{Po}$  in the crystal surface that ends with 1.2 MeV. Since we use the coincidence events there is no significant chance to the coincide in both crystals by the backgrounds from the PMTs that is the main contributor to the external background. As a result of the fit, the mean of the exponential depth distribution with  $p_3$  is as shallow as  $(0.107 \pm 0.003) \mu\text{m}$ . The ratio of the amplitudes of two exponential distributions,  $p_0$  to  $p_2$ , is approximately 0.76; therefore, the depth distribution of  $^{210}\text{Pb}$  in the surface of an NaI(Tl) crystal consists of both shallow and deep depth profiles.

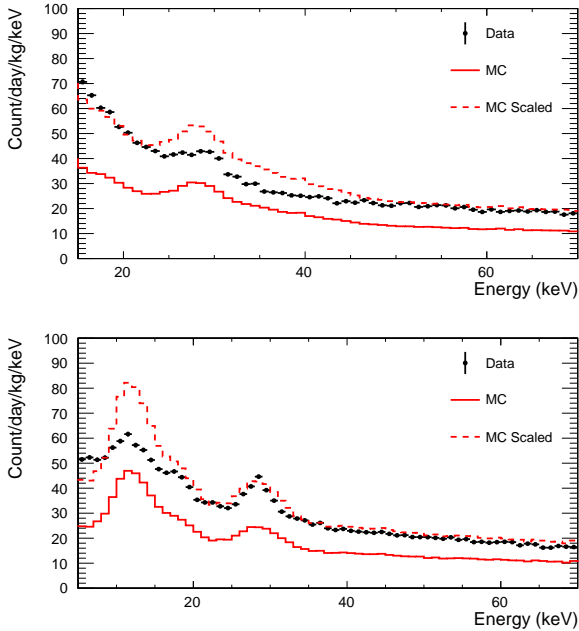


Figure 7: Low-energy spectra due to the beta decay of  $^{210}\text{Pb}$  generated in the surface with the mean-depth parameter,  $p_1$ , including all the energy deposited in the clean Crystal A (bottom) and in the contaminated Crystal B (top). The energy spectra are compared with the measurement results (filled black circles). Dashed line: scaled spectrum (see text).

According to the decay chain for  $^{210}\text{Pb}$ , most events with energy deposition in the crystals are attributed to the conversion electrons, Auger electrons, and  $\gamma$ /X-rays, followed by the beta electrons from the decay to  $^{210}\text{Bi}$  of  $^{210}\text{Pb}$  in the surface of Crystal B. Therefore, the coincidence events might possess an energy correlation between Crystals A and B. In Fig. 9, we depict a scatter plot of the energy deposition in Crystal A versus that in Crystal B. Figure 9(a), (b), and (c) depict the simulated results both without including a DL and upon including a DL, respectively; Fig. 9(d) depicts the measured data. In the simulation, because it is found to be in good agreement with the data when it is dominated by 3 and 4- $\mu\text{m}$  thick DLs in the fit, we included 3 and 4- $\mu\text{m}$  thick DLs while generating  $^{210}\text{Pb}$  decays at random locations within the surface thickness of  $0.5 \mu\text{m}$  in the contaminated Crystal B; subsequently, we reproduced the distinct islands at approximately 20 and 30 keV in one crystal and at 30 and 20 keV in the other one, as evident from the measured data, while the islands are not depicted in Fig. 9(a), which does not consider a DL.

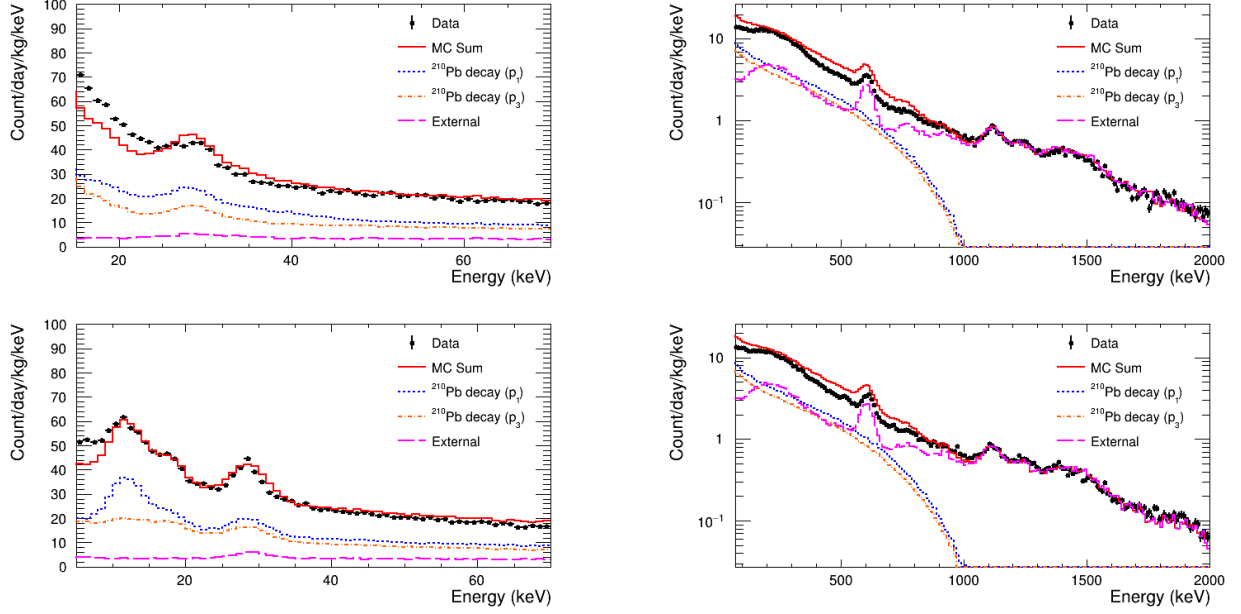


Figure 8: Fitted energy spectra for both Crystals A (bottom) and B (top) are compared with the measurement results (black circles). The left ones represent the low-energy spectra and the right ones the high-energy spectra of the beta-decay events.

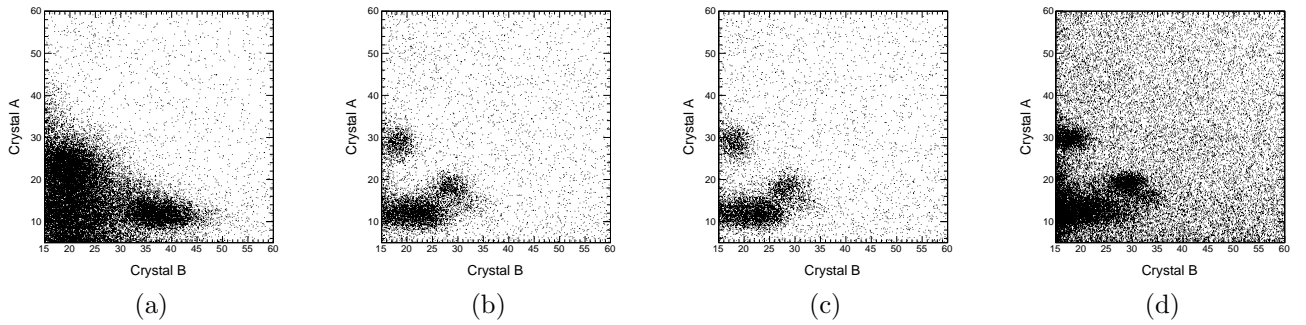


Figure 9: Energy deposited in Crystal A versus that deposited in Crystal B (in units of keV). (a), (b), and (c) represent the simulated results and (d) the measured data. We generated the  $^{210}\text{Pb}$  decays at random locations within the surface thickness of  $0.5\ \mu\text{m}$  in the contaminated Crystal B both without a DL (a), with a  $3\text{-}\mu\text{m}$  thick DL (b), and with a  $4\text{-}\mu\text{m}$  thick DL (c).



## 5. Conclusion

We have studied the depth profile of the surface  $^{210}\text{Pb}$  contamination of an NaI(Tl) crystal by modeling the measured energy spectra with the simulated spectra using the Geant4 toolkit. We first fitted the alpha-decay events with the simulated spectrum from the alpha decay of  $^{210}\text{Po}$  that is exponentially distributed within the crystal surface by following an exponential function under the presence of an inactive region; subsequently, we showed that the fitted result was in good agreement with the alpha data. In addition, to improve the depth profile for shallow depths below  $1\text{ }\mu\text{m}$ , we studied the energy spectrum from the beta decay of  $^{210}\text{Pb}$  whose spectral features were attributed to  $\gamma$ /X-rays and conversion electrons that were mainly distributed within shallow depths. Subsequently, we showed that all the fitted results of both the clean and contaminated crystals were in good agreement with the data for both the low- and high-energy events.

Using this study, we can provide the quantitative understanding of the depth profile of the surface  $^{210}\text{Pb}$  contamination in an NaI(Tl) crystal exposed to  $^{222}\text{Rn}$ . Furthermore, our analysis method and results can be applied to NaI(Tl) experiments, in general, to describe the backgrounds in case of  $^{210}\text{Pb}$  surface contamination. Since the low-energy spectral feature due to the beta decays of the surface  $^{210}\text{Pb}$  contamination is primarily attributed to depth profiles of  $^{210}\text{Pb}$  distributed within a shallow surface with the mean depth of  $0.107\text{ }\mu\text{m}$  as well as a deep surface with mean depth of  $1.39\text{ }\mu\text{m}$ , it is expected to be similar for depth profiles of the surface  $^{210}\text{Pb}$  in different crystals. However, it could be affected by the  $^{222}\text{Rn}$  exposure. There is also the possibility of bulk  $^{210}\text{Pb}$  contamination, which is expected to affect the low-energy spectrum and, thus, the  $^{210}\text{Pb}$  contribution is estimated by modeling the background from bulk  $^{210}\text{Pb}$  and surface  $^{210}\text{Pb}$ .

## Acknowledgments

We thank the Korea Hydro and Nuclear Power Company for providing underground laboratory space at Yangyang. This work was supported by the Institute for Basic Science (South Korea) under project code IBS-R016-A1.

## References

- [1] E. Komatsu *et al.* (WMAP Collaboration), *Astrophys. J. Suppl.* 192 (2011) 18.
- [2] P. A. R. Ade *et al.* (Planck Collaboration), arXiv:1303.5076.
- [3] B. W. Lee and S. Weinberg, *Phys. Rev. Lett.* 39 (1977) 165.
- [4] G. Jungman, A. Kamionkowski, G. Griest, *Phys. Rep.* 267 (1996) 195.
- [5] R. Gaitskell, *Annu. Rev. Nucl. Part. Sci.* 54 (2004) 315.
- [6] L. Baudis, *Phys. Dark Univ.* 1 (2012) 94.
- [7] R. Bernabei, DAMA collaboration, *Eur. Phys. J. C* 56 (2008) 333; R. Bernabei *et al.* (DAMA Collaboration), *Eur. Phys. J. C* 67 (2010) 39; R. Bernabei *et al.* (DAMA Collaboration), *Eur. Phys. J. C* 73 (2013) 2648.
- [8] G. Adhikari, *et al.* (COSINE-100 collaboration), Search for a dark matter-induced annual modulation signal in NaI(Tl) with the COSINE-100 experiment, *Phys. Rev. Lett.* 123, 031302 (2019).
- [9] E. Barbosa de Souza *et al.*, First search for a dark matter annual modulation signal with NaI(Tl) in the Southern Hemisphere by DM-Ice17, *Phys. Rev. D* 95 (3) (2017) 032006. doi:10.1103/PhysRevD.95.032006.
- [10] J. Amaré *et al.*, First results on dark matter annual modulation from ANAIS-112 experiment, *Phys. Rev. Lett.* 123 (2019) 031301.
- [11] M. Antonello *et al.*, The SABRE project and the SABRE Proof-of-Principle, *Eur. Phys. J. C* 79 (2019) 363.
- [12] K. Fushimi, *et al.*, Dark matter search project PICO-LON, *J. Phys. Conf. Ser.* 718 (4) (2016) 042022. doi:10.1088/1742-6596/718/4/042022.
- [13] G. Angloher *et al.*, The COSINUS project: perspectives of a NaI scintillating calorimeter for dark matter search, *Eur. Phys. J. C* 76 (2016) 441.
- [14] R. Bernabei, *et al.*, Final model independent result of DAMA/LIBRA-phase1, *Eur. Phys. J. C* 73 (2013) 2648. doi:10.1140/epjc/s10052-013-2648-7.
- [15] R. Bernabei, *et al.*, First model independent results from DAMA/LIBRA-Phase2, *Nucl. Phys. At. Energy* 19 (2018) 307, arXiv:1805.10486 [astro-ph.IM].
- [16] S. Agostinelli, GEANT4: a simulation toolkit, *Nucl. Instrum. Meth. A* 506 (2003) 250, doi:10.1016/S0168-9002(03)01368-8.
- [17] P. Adhikari *et al.* (COSINE-100 collaboration), Understanding NaI(Tl) crystal background for dark matter searches, *Eur. Phys. J. C* 77 (2017) 437.
- [18] P. Adhikari *et al.* (COSINE-100 collaboration), Background model for the NaI(Tl) crystals in COSINE-100, *Eur. Phys. J. C* 78 (2018) 490, doi:10.1140/epjc/s10052-018-5970-2.
- [19] E. Barbosa de Souza, *et al.* (COSINE-100 collaboration), Study of cosmogenic radionuclides in the COSINE-100 NaI(Tl) detectors, *Astropart. Phys.* 115 (2020) 102390.
- [20] J. Amaré, *et al.*, Analysis of backgrounds for the ANAIS-112 dark matter experiment, *Eur. Phys. J. C* 79 (2019) 412.
- [21] J. Amaré, *et al.*, Assessment of backgrounds of the ANAIS experiment for dark matter direct detection, *Eur. Phys. J. C* 76 (2016) 429.
- [22] S. Cebrian, *et al.*, Background model for a NaI (Tl) detector devoted to dark matter searches, *Astropart. Phys.* 37 (2012) 60.
- [23] N. J. T. Smith, J. D. Lewin, P. F. Smith, A possible mechanism for anomalous pulses observed in sodium iodide crystals, *Phys. Lett. B* 485 (2000) 9.
- [24] S. Cooper, H. Kraus, J. Marchese, Radon-implanted  $^{214}\text{Po}$  and anomalous pulses in sodium iodide detectors for dark matter, *Phys. Lett. B* 490 (2000) 6.
- [25] R. Agnese, *et al.*, Demonstration of surface electron rejection with interleaved germanium detectors for dark matter searches, *Appl. Phys. Lett.* 103, 164105 (2013).
- [26] R. Agnese, *et al.*, Projected sensitivity of the SuperCDMS SNOLAB experiment, *Phys. Rev. D* 95 (2017) 082002.
- [27] R. Strauss, *et al.*, A detector module with highly efficient surface-alpha event rejection operated in CRESST-II Phase 2, *Eur. Phys. J. C* 75 (2015) 352.
- [28] G. Adhikari, *et al.*, Initial performance of the COSINE-100 Experiment, *Eur. Phys. J. C* 78 (2018) 107. doi:10.1140/epjc/s10052-018-5590-x.
- [29] G. Adhikari, *et al.*, An experiment to search for dark-matter interactions using sodium iodide detectors, *Nature* 564 (7734) (2018) 83–86. doi:10.1038/s41586-018-0739-1.
- [30] S. C. Kim *et al.*, New Limits on Interactions between Weakly Interacting Massive Particles and Nucleons Obtained with CsI(Tl) Crystal Detectors, *Phys. Rev. Lett.* 108 (2012) 181301, [1204.2646].
- [31] K. W. Kim *et al.*, Measurement of low-energy events due to  $^{222}\text{Rn}$  daughter contamination on the surface of a NaI(Tl) crystal, *Astropart. Phys.* 02 (2018) 51, [1801.06948].
- [32] R. Bernabei *et al.*, The DAMA/LIBRA apparatus, *Nucl. In-*

strum. Meth. A 592 (2008) 297.

- [33] Pin Yang, Charles D. Harmon, F. Patrick Doty, and James A. Ohlhausen, Effect of humidity on scintillation performance in Na and Tl activated CsI crystals, IEEE Trans. Nucl. Sci. 61 (2) 2014.